Magnetochemistry **2015**, *1*, 62-71; doi:10.3390/magnetochemistry1010062

OPEN ACCESS

magnetochemistry

ISSN 2312-7481

www.mdpi.com/journal/magnetochemistry

Article

Magnetic Behaviour of Transition Metal Complexes with Functionalized Chiral and C_{60}-Filled Nanotubes as Bridging Ligands: A Theoretical Study

Silvia Gómez-Coca and Eliseo Ruiz *

Departament de Química Inorgànica and Institut de Recerca de Química Teòrica i Computacional, Universitat de Barcelona, Diagonal 645, Barcelona E-08028, Spain; E-Mail: silvia.gomez@qi.ub.es

* Author to whom correspondence should be addressed; E-Mail: eliseo.ruiz@qi.ub.es; Tel.: +34-934-037-058.

Academic Editor: Carlos J. Gómez García

Received: 3 November 2015 / Accepted: 19 November 2015 / Published: 4 December 2015

Abstract: Functionalized nanotubes are promising candidates to promote communication between paramagnetic centres at large distances through their highly delocalized π systems. Here, Density Functional Theory methods are employed to study the exchange coupling interaction between Fe^{III} paramagnetic centres coordinated at terminal carboxylate ligands of functionalized nanotubes. Chiral nanotubes exhibit ferromagnetic coupling at long distances while non-chiral systems usually favor antiferromagnetic coupling. The inclusion of C_{60} molecules inside the nanotube, resulting in peapod structures, in some cases causes dramatic changes in the coupling interactions and spin density.

Keywords: carbon nanotubes; magnetic properties; density functional theory; metal functionalization

1. Introduction

Carbon nanotubes have been extensively employed in recent years for many purposes [1]. One of the most developed applications is the use of single carbon nanotubes in electronic devices and sensors [2]. The most interesting feature of such devices is that electrons can flow through the nanotube and consequently, the nanotube conductivity can be modified by the adsorption of chemical species to the nanotube wall [3]. The conductivity of the carbon nanotubes, semiconducting or metallic, is directly

related to their chirality and their characteristic band structure. Related to these properties is the capacity of the carbon nanotubes to "communicate" electronically between the two ends. Actually, for a system with two paramagnetic centres, single-molecule conductivity and exchange coupling should be related. Thus, at first glance, strong antiferromagnetic coupling should be present in systems with high conductivity. However, this assumption is not always the case for real systems. Carbon nanotubes can be described as grapheme sheets wrapped into cylinders with a carbon atom superposed at each end. The vector defined by the two superposed atoms can by described using a pair of integer indices (n,m) indicating the number of unit vectors in the honeycomb graphene lattice. Thus, $n = m$ or $m = 0$ correspond to zigzag or armchair nanotubes that are non-chiral, while the other possible (n,m) values result in chiral nanotubes. Prior to this work, we theoretically explored the exchange interactions between paramagnetic centres (Fe^{III} cations) coordinated to non-chiral functionalized carbon nanotubes through carboxylate groups (see coordination mode in Figure 1) [4]. This nanotube functionalization is one of the most common because terminal carboxylate groups can be incorporated into the nanotubes by treating them with a range of different oxidants [5]. In addition, the presence of the carboxylate groups improves the solubility of the nanotubes and makes them amenable to chemical reactions. Our results indicated that at very long distances, relatively large exchange coupling interactions can be achieved by using functionalized carbon nanotubes as bridging ligands. For instance, a value of $J = -89.0$ cm^{-1} was calculated for a distance between the Fe^{III} centres of 76.1 Å with a functionalized (5,5) carbon nanotube, where the nature of the coupling was antiferromagnetic in all cases. The main goal of this paper is to extend our previous study to the magnetic properties of dinuclear metal complexes with chiral single-wall carbon nanotubes (SWNTs) and peapod systems as bridges, using theoretical methods based on density functional theory (DFT).

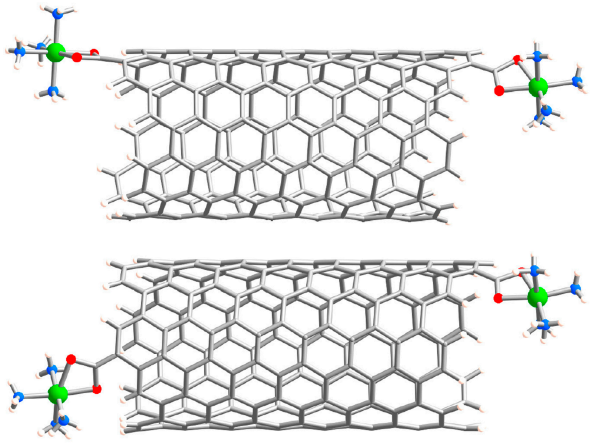

Figure 1. Representation of the two different (7,6) carboxylate-functionalized SWNT-Fe^{III} models employed in the calculations. The right terminal group remains fixed while the left one is modified to examine the influence of the relative position of the two Fe^{III} centres.

2. Results and Discussion

2.1. Metal Systems with Chiral Nanotubes

In order to study the exchange coupling between paramagnetic centres through nanotubes, we selected some metallic and some semiconducting chiral nanotubes coordinated through terminal carboxylate

groups with Fe^{III} cations and with a high-spin d^5 configuration. The Fe^{III} centres were selected as the d^5 configuration provides the maximum number of unpaired electrons. In addition, the charge of +3 results in stronger mixing with the nanotube orbitals than an equivalent Mn^{II} complex because the projected density of states (DOS) of the occupied 3d orbitals of the iron Fe^{III} cations (between −15 and −7 eV) are closer in energy to the contributions to the total DOS of the occupied π orbitals of the nanotube carbon atoms (see Figure 2). This enhances the exchange interactions between the paramagnetic Fe^{III} centres. Furthermore, we added ammonia molecules to complete the coordination sphere of the transition metal atoms; then we assumed that the carboxylate groups act as chelating ligands (see models for the (7,6) nanotube in Figure 1) and that the dangling bonds of the terminal nanotube carbon atoms that are not functionalized were suppressed by the inclusion of hydrogen atoms.

Table 1 shows the *J* values for the models studied, calculated using DFT. Their analysis allowed us to extract the following conclusions: (i) Most of the chiral nanotubes give ferromagnetic coupling; (ii) There is no simple relationship between the nature of the exchange interaction and the chirality, (*n*,*m*), diameter and conductivity behaviour that depends on the modulus of (*n*−*m*,3) value (0 metallic and 1, 2 semiconductor) of the nanotube, as can be seen in Table 1 and Figure 3; (iii) Changing the relative positions of the terminal carboxylate groups coordinated to the paramagnetic Fe^{III} centres does not significantly change the *J* value calculated. This agrees with our previous calculations for a (5,5) model nanotube complex: independently of the relative position of the terminal carboxylate groups, the Fe···Fe exchange coupling was always antiferromagnetic. Hence, the nature of the exchange interaction is a characteristic feature of each nanotube chirality; (iv) The increase of the Fe···Fe distance in the (10,7) nanotube enhances the ferromagnetic interaction. For the (5,5) nanotube, the increased distance from 25.2 to 76.1 Å resulted in a diminution of the antiferromagnetic coupling from −255.6 to −89.0 cm^{-1}; (v) Antiferromagnetic coupling is stronger than ferromagnetic coupling. Thus, we can conclude that the chirality of the nanotubes can induce ferromagnetic coupling while the previously studied non-chiral systems were antiferromagnetic.

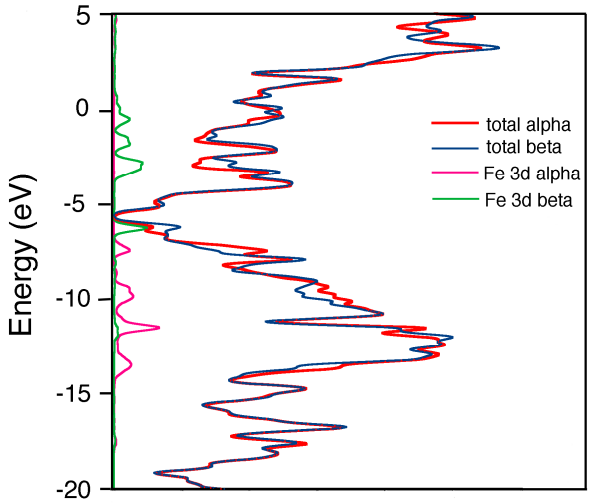

Figure 2. Representation of the total density of states and of the contribution of the d orbitals of the iron atoms (alpha and beta contributions) of the (7,6) carboxylate-functionalized SWNT-Fe^{III} model shown above in Figure 1.

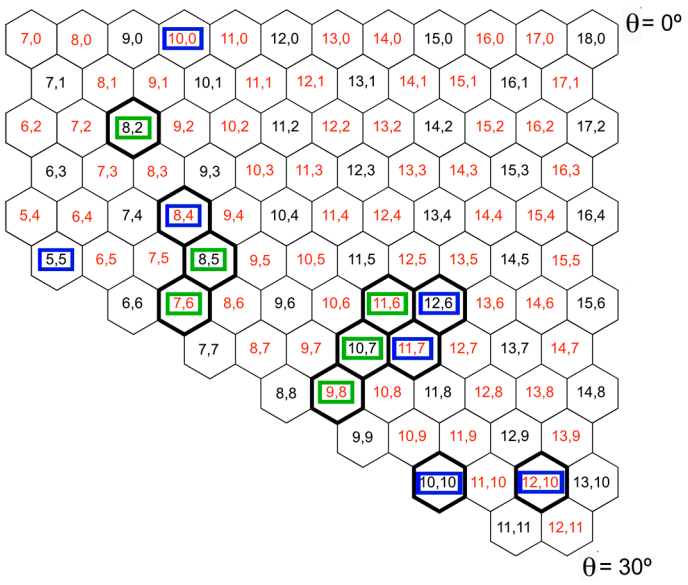

Figure 3. Dependence of the exchange coupling constants on the chirality and charge transport properties of the carbon nanotubes. The (*n*,*m*) indices are written in black and red for metallic and semiconductor nanotubes, respectively. Blue and green rectangles represent antiferromagnetic and ferromagnetic calculated *J* values, respectively. Hexagons in bold are the nanotubes calculated in this work.

Table 1. Chirality, diameter (in Å and calculated using a C–C bond length of 1.42 Å) and the corresponding charge transport properties (SC: semiconductor, M: metallic) for the carbon nanotubes functionalized with terminal carboxylate groups coordinated to Fe^{III} centres. *J* values (in cm^{-1}) for the coupling of the two Fe^{III} cations and the distance (in Å) between them calculated using DFT. Cases with more than one calculated *J* value correspond to coordination of the Fe^{III} cations to different terminal carboxylate groups of the nanotube (see Figure 1).

Chirality	Transport	Diameter	*d*(Fe···Fe)	J_{calc}
(7,6)	SC	8.82	25.4, 25.9	+17.2, +19.3
(8,2)	M	7.18	31.1, 32.4	+9.0, +11.0
(8,4)	SC	8.29	25.9, 25.6	−230, −260
(8,5)	M	8.89	25.7, 26.2	+21.3, +28.6
(9,8)	SC	11.53	38.8	+6.1
(10,7)	M	11.59	40.2, 26.7	+94.8, +13.6
(10,10)	M	13.56	40.91	−17.6
(11,6)	SC	11.69	40.2	+11.7
(11,7)	SC	12.30	40.1	−150
(12,6)	M	12.43	38.8	−22.0
(12,10)	SC	14.94	47.51	−199

Spin distributions corresponding to the ferromagnetic solutions of the complexes studied are represented in Figure 4 and Figure S1. There is a predominance of the delocalization mechanism in the atoms neighbouring the Fe^{III} centres. Due to the presence of two unpaired electrons in the antibonding e_g orbitals there is relatively extensive orbital mixing with the ligands and, consequently, the sign of the

spin density in such atoms is equal that in the metal. In the carbon atoms of the nanotube, the predominant mechanism should be spin polarization. However, there is not always a clear spin density sign distribution pattern. In many areas of the nanotubes, it is possible to identify the typical alternation of signs between neighbouring atoms due to the spin polarization mechanism. Basically, there are relatively large positive contributions in one atom (blue lobe) while the neighbouring atoms have a smaller negative spin population (white lobe, in many cases not shown in the figure due to the threshold value chosen). Comparative analysis of the ferromagnetic and antiferromagnetic systems showed no significant differences either at the qualitative level in the plotted spin densities (Figure 4 and Figure S2) or at the quantitative level in the calculated atomic spin population values (not shown).

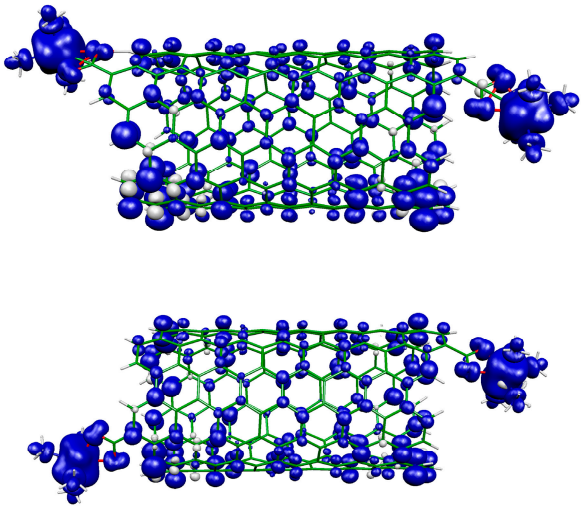

Figure 4. Representation of the spin distribution for the ferromagnetic solution of the Fe^{III} complex-(7,6) SWNT models (see Figure 1). Dark and clear regions indicate positive and negative spin populations, respectively. The isodensity surface shown corresponds to a value of 0.001 e^{-}/bohr^3 (see Figure S1 for the equivalent plot for the other models studied).

2.2. Systems Based on Peapods

We also extended our study to peapods, in order to examine the possible role of the C_{60} units placed inside the nanotube cavity in the exchange interaction between the terminal Fe^{III} centres. Such peapod structures take profit of the nanocapillarity behavior of carbon nanotubes [6] to fill them with fullerenes. Thus, Table 2 shows some of the *J* values calculated for the empty nanotubes together with those for the equivalent peapod. The C_{60} molecules were shifted inside the cavity (1 Å in 0.2 Å steps) with no significant differences (around 1–2 cm^{-1}, see Supplementary Materials Table S1) in the calculated *J* values.

Analysis of the *J* values shows that only in the case of the (10,10) system is there a notable change in the nature of the magnetic coupling due to the inclusion of the C_{60} molecules. In the (10,7) nanotube, the *J* value diminishes with the inclusion of the C_{60} molecules; and in the other nanotubes, the *J* values only vary slightly. As the diameter of C_{60} is 7.11 Å and the distance between two graphite layers is 3.35 Å, there is a critical nanotube diameter of approximately 12.8 Å beyond which the interaction is exothermic [7]. We have calculated the interaction energy between the functionalized nanotube with the two Fe^{III} centres and the three C_{60} molecules. As expected, the interaction energy is positive

(endothermic) for nanotubes with smaller diameters and becomes larger as the diameter is reduced. From nanotube (10,10), the interaction energy starts to be favourable. However, that does not explain the behaviour of the (10,10) nanotube because nanotube (12,10) presents a similar exchange interaction before and after the inclusion of C_{60} molecules. The analysis of the spin density (see Figure 5) and the density of states (not shown) for the (10,10) nanotube with and without C_{60} molecules does not present any significant differences that could explain the observed behaviour.

Table 2. Chirality, diameter (in Å) and the corresponding charge transport properties (SC: semiconductor, M: metallic) for the carbon nanotubes functionalized with terminal carboxylate groups coordinated to Fe^{III} centres. *J* values (in cm^{-1}) for the coupling of the two centres and the distance (in Å) between them for the nanotube-Fe^{III} complex calculated using DFT. *J* values calculated for the equivalent peapod-Fe^{III} complex when filling the nanotube structure with three C_{60} molecules (diameter 7.11 Å). Interaction energy (E_{inter}) between the three C_{60} molecules and the functionalized nanotube ($E_{inter} = E_{system} - E_{nanotube} - E_{3C60}$ in eV).

Chirality	Transport	Diameter	*d*(Fe···Fe)	J_{nano}	J_{peapod}	E_{inter}
(9,8)	SC	11.53	38.8	+6.1	+18.2	58.9
(10,7)	SC	11.59	40.2	+94.8	+15.4	52.9
(11,6)	SC	11.69	40.2	+11.7	+7.0	44.0
(11,7)	SC	12.30	40.1	−150	−143	13.8
(12,6)	M	12.43	38.8	−22.0	−33.9	10.3
(10,10)	M	13.56	40.91	−17.6	+43	−1.9
(12,10)	SC	14.94	47.51	−199	−182	−2.0

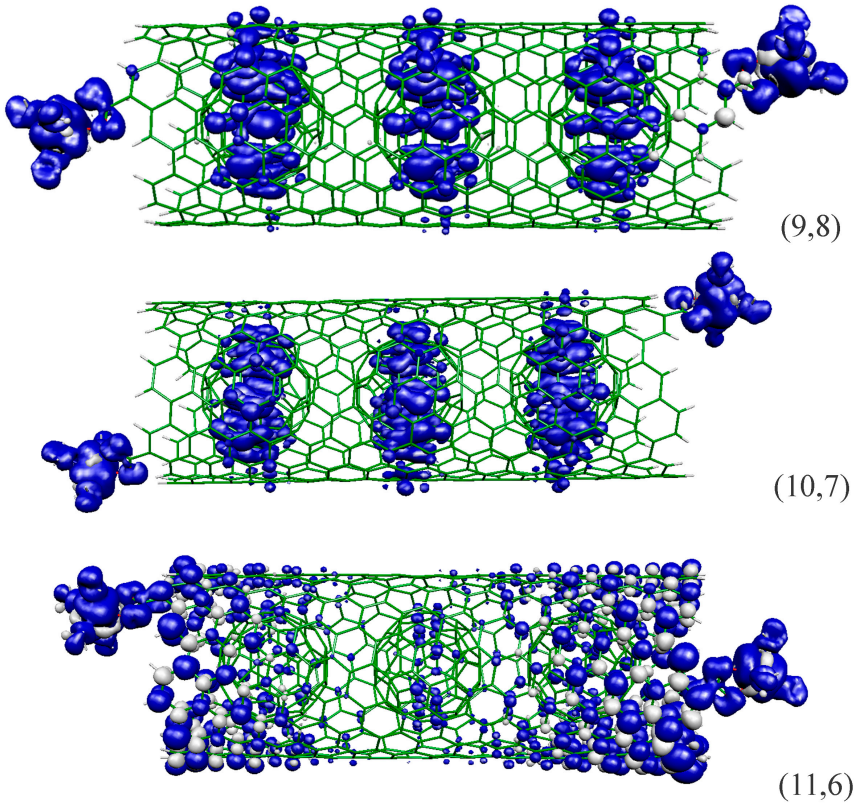

Figure 5. *Cont.*

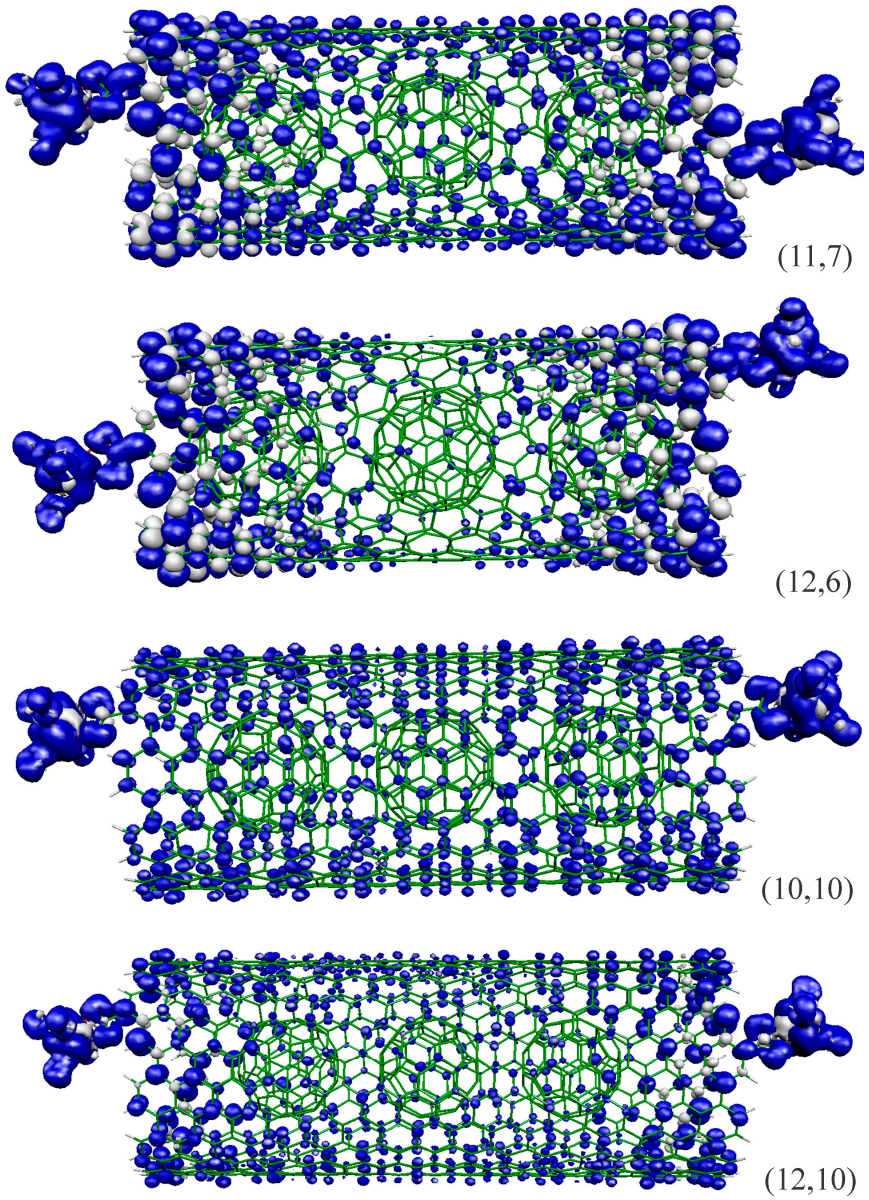

Figure 5. Spin distribution for the ferromagnetic solution of the Fe^{III} complex-peapod models. Clear and dark isodensity surfaces indicate positive and negative spin populations, respectively, with a value of 0.0004 e^{-}/bohr^3 for the (9,8) nanotube and, for the other nanotubes, it diminished in proportion of the number of atoms of carbon (for comparison).

The spin density plots for the different peapods (see Figure 5) reveal a large delocalization of the positive spin density from the nanotube to the C_{60} molecules in the (9,8) and (10,7) peapods: the nanotubes with the smallest diameters. However, in the case of the (11,6) peapod (with a slightly larger diameter), there is only a small contribution to the spin density from the C_{60} molecules. There is probably a critical nanotube diameter at which the small distance between the C_{60} and the nanotube walls leads to a large spin delocalization from the nanotube to the C_{60} molecule. Finally, it is worth noting that the inclusion of dispersion terms in the DFT calculations [8] does significantly change neither the values of the calculated *J* values nor the spin population analysis.

3. Computational Details

Electronic structure calculations were carried out using the SIESTA (Spanish Initiative for Electronic Simulations with Thousands of Atoms) code [9–12]. This computer code is highly efficient when dealing with systems that contain a large number of atoms and therefore for those studied here. The generalized-gradient approximation (GGA) functional expression of Perdew, Burke and Ernzerhof (PBE) [13] was employed and pseudopotentials were generated according to the method suggested by Trouiller and Martins [14]. A triple-ζ numerical basis set with polarization functions for the iron atoms was employed, while a double-ζ basis with polarization functions was used for the other elements. Values of 50 meV for the energy shift and 250 Ry for the mesh cutoff provide a good compromise between accuracy and the computational cost of estimating the exchange coupling constants, according to a previous study [15]. To calculate the exchange coupling constants, we employed the Heisenberg Hamiltonian $\hat{H} = -J\hat{S}_1\hat{S}_2$ and a detailed description of the procedure used to obtain the exchange coupling constants can be found in previous papers [16,17]. Spin-orbit effects were not considered due to the light atoms of the nanotubes and the isotropic electron distribution of the Fe^{III} cations. The metallic nature of some carbon nanotubes [18] together with the presence of paramagnetic centers makes the convergence of such calculations quite challenging. The model structures were not optimized and we employed the following structural parameters: *d*(C–C) = 1.42 Å, *d*(C–O) = 1.37 Å, *d*(Fe–O) = 2.077 Å, *d*(Fe–N) = 2.05 Å, *d*(N–H) = 0.9 Å, *d*(C–H) = 1.1 Å, O–C–O angle = 110° and N–Fe–N angle = 90°. In order to check if the optimization of the nanotube structures could change the calculated *J* values, we performed the optimization of the (7,6) nanotube system (see Supplementary Materials) and the calculated varies slightly.

4. Conclusions

Previously, we studied exchange interactions between two paramagnetic metal centres through zigzag and armchair types of single-wall carbon nanotubes and observed antiferromagnetic coupling through the nanotube. Here, we extend the study to both metallic and semiconducting chiral nanotubes, as well as, in some cases, inserting fullerenes to produce peapod structures. For this study, in order to calculate the exchange coupling constant between Fe^{III} cations, we employed the SIESTA program with the PBE exchange-correlation functional. From calculated *J* values for the different nanotubes some conclusions can be drawn: (i) Most chiral nanotubes show ferromagnetic coupling. Furthermore, if the coupling is antiferromagnetic, its magnitude is greater than that of the equivalent complexes with non-chiral nanotubes. (ii) There is no clear relationship between the values of *J* obtained and the chirality or conductivity of the nanotubes. Taking into account the relatively large calculated values, the lack of correlation cannot be attributed to deficiencies of the computational approach. (iii) The relative positions of the metal centres do not substantially affect the exchange interactions. Furthermore, the use of optimized or partially optimized structures also lead to similar calculated *J* values (see Supplementary Materials).

The plotted spin densities of the ferromagnetic solutions of the complexes show that between the metal cation and its neighbouring atoms, the predominant spin relaxation mechanism is spin delocalization due to the presence of two electrons in the antibonding orbitals: e_g Fe^{III} orbitals mix extensively with antibonding ligand orbitals resulting in a spin density of the same sign in these atoms.

However, the nanotube is controlling the polarization mechanism as is clearly reflected by the typical pattern of alternating signs (a large positive contribution in one atom and a small negative one in the neighbour). For larger nanotubes, the study was extended by introducing three fullerenes inside the nanostructure. Only one case (10,10) showed a qualitative change in the sign of the exchange coupling. In the case of the (10,7) system, there is a considerable decrease of the ferromagnetic coupling. Further analysis of the spin density revealed delocalization of the spin density of the fullerene nanotube. One possible cause of this unusual behaviour could be the smaller diameter; for instance, the equivalent system with the (11,6) nanotube has a very similar diameter, but the spin density in the internal fullerenes was not delocalized.

Supplementary Materials

Figure S1 including the spin distributions of the studied SWNTs. Figure S2 comparison optimized and model structure of (7,6) nanotube. Table S1 *J* values with shift of C60 molecules inside (11,6) and (9,8) nanotubes.

Acknowledgments

S.G.C. thanks the Spanish *Ministerio de Educación, Cultura y Deporte* for a predoctoral fellowship. E.R. thanks Generalitat de Catalunya for an ICREA Academia Fellowship. The authors acknowledge the computer resources, technical expertise and assistance provided by the Barcelona Supercomputing Centre.

Author Contributions

S.G.C. performed the calculations. S.G.C. and E.R. conceived and designed the experiments. S.G.C. and E.R. wrote the paper.

Conflicts of Interest

The authors declare no conflict of interest.

References

1. Dresselhaus, M.S.; Dresselhaus, D.; Avouris, G. *Carbon Nanotubes: Synthesis, Structure, Properties and Applications*; Springer-Verlag: Berlin, Germany, 2001.
2. Schnorr, J.M.; Swager, T.M. Emerging applications of carbon nanotubes. *Chem. Mater.* **2011**, *23*, 646–657.
3. Anantram, M.P.; Leonard, F. Physics of carbon nanotube electronic devices. *Rep. Prog. Phys.* **2006**, *69*, 507–561.
4. Ruiz, E.; Nunzi, F.; Alvarez, S. Magnetic communication through functionalized nanotubes: A theoretical study. *Nano Lett.* **2006**, *6*, 380–384.
5. Liu, J.; Rinzler, A.G.; Dai, H.J.; Hafner, J.H.; Bradley, R.K.; Boul, P.J.; Lu, A.; Iverson, T.; Shelimov, K.; Huffman, C.B.; *et al.* Fullerene pipes. *Science* **1998**, *280*, 1253–1256.

6. Pederson, M.R.; Broughton, J.Q. Nanocapillarity in fullerene tubules. *Phys. Rev. Lett.* **1992**, *69*, 2689–2692.
7. Okada, S.; Saito, S.; Oshiyama, A. Energetics and electronic structures of encapsulated C_{60} in a carbon nanotube. *Phys. Rev. Lett.* **2001**, *86*, 3835–3838.
8. Dion, M.; Rydberg, H.; Schröder, E.; Langreth, D.C.; Lundqvist, B.I. Van der Waals Density Functional for General Geometries. *Phys. Rev. Lett.* **2004**, *92*, 246401.
9. Sánchez-Portal, D.; Ordejón, P.; Artacho, E.; Soler, J.M. Density-functional method for very large systems with LCAO basis sets. *Int. J. Quantum Chem.* **1997**, *65*, 453–461.
10. Artacho, E.; Sánchez-Portal, D.; Ordejón, P.; García, A.; Soler, J.M. Linear-scaling ab-initio calculations for large and complex systems. *Phys. Status Solidi A* **1999**, *215*, 809.
11. Artacho, E.; Anglada, E.; Diéguez, O.; Gale, J.D.; García, A.; Junquera, J.; Martin, R.M.; Ordejón, P.; Pruneda, J.M.; Sánchez-Portal, D. The siesta method; developments and applicability. *J. Phys.: Condens. Matter* **2008**, *20*, 064208.
12. Soler, J.M.; Artacho, E.; Gale, J.D.; García, A.; Junquera, J.; Ordejón, P.; Sánchez-Portal, D. The siesta method for *ab initio* order-*N* materials simulation. *J. Phys.: Condens. Matter* **2002**, *14*, 2745.
13. Perdew, J.P.; Burke, K.; Ernzerhof, M. Generalized gradient approximation made simple. *Phys. Rev. Lett.* **1996**, *77*, 3865–3868.
14. Troullier, N.; Martins, J.L. Efficient pseudopotentials for plane-wave calculations. *Phys. Rev. B* **1991**, *43*, 1993.
15. Ruiz, E.; Rodriguez-Fortea, A.; Tercero, J.; Cauchy, T.; Massobrio, C. Exchange coupling in transition-metal complexes via density-functional theory: Comparison and reliability of different basis set approaches. *J. Chem. Phys.* **2005**, *123*, 074102.
16. Ruiz, E.; Alvarez, S.; Cano, J.; Polo, V. About the calculation of exchange coupling constants using density-functional theory: The role of the self-interaction error. *J. Chem. Phys.* **2005**, *123*, 164110.
17. Ruiz, E.; Rodriguez-Fortea, A.; Cano, J.; Alvarez, S.; Alemany, P. About the calculation of exchange coupling constants in polynuclear transition metal complexes. *J. Comput. Chem.* **2003**, *24*, 982–989.
18. Mintmire, J.W.; Dunlap, B.I.; White, C.T. Are fullerene tubules metallic? *Phys. Rev. Lett.* **1992**, *68*, 631–634.